PAPER

Check for updates

Automated cellular stimulation with integrated pneumatic valves and fluidic capacitors†

Damilola I. Adeoye, [iD] [a] Yao Wang, [iD] [a] Joshua J. Davis[a] and Michael G. Roper [iD] *[a,b]

Microfluidic technologies have proven to be a reliable tool in profiling dynamic insulin secretion from islets of Langerhans. Most of these systems rely on external pressure sources to induce flow, leading to difficulties moving to more elaborate systems. To reduce complexity, a microfluidic system was developed that used a single vacuum source at the outlet to drive fluidic transport of immunoassay reagents and stimulation solutions throughout the device. A downside to this approach is the lack of flow control over the reagents delivered to the islet chamber. To address this challenge, 4-layer pneumatic valves were integrated into the perfusion lines to automate and control the delivery of stimulants; however, it was found that as the valves closed, spikes in the flow would lead to abnormal insulin secretion profiles. Fluidic capacitors were then incorporated after the valves and found to remove the spikes. The combination of the valves and capacitors resulted in automated collection of insulin secretion profiles from single murine islets that were similar to those previously reported in the literature. In the future, these integrated fluidic components may enable more complex channel designs to be used with a relatively simple flow control solution.

Introduction

Plasma glucose homeostasis is regulated by a number of hormones secreted by islets of Langerhans, micro-organs in the pancreas composed of several types of cells.[1] For example, insulin is secreted from β-cells in response to elevated glucose in a biphasic pattern with a large burst in the first 10–15 min followed by a period of sustained release.[2–4] The secretion patterns of the various hormones are essential for maintaining euglycemia and defective secretion is a hallmark of diabetes.[4]

Because of the importance of proper insulin secretion, this parameter is often used to evaluate and screen islet function in pre-transplant evaluation for type 1 diabetes therapy.[5] To increase the ease of screening of islet function, several microfluidic devices have been developed.[6–14] To increase throughput while simplifying flow control, vacuum-based fluidic transport can be used.[15–19] Typically, a single vacuum line is applied to the outlet of the device and the resistances of each channel determine the flow rates. Active control from one or several channels in this type of system is more difficult to achieve. For example, in the devices that have used vacuum-based transport for examining secretion from islets, no active control over the flow in any of the channels was reported.[16–18] This lack of control required manual replacement of solutions that changed composition over time, for example, perfusion solutions that contained different glucose concentrations to stimulate islets. In addition to being cumbersome, increased manual manipulation can lead to contamination of the device or reagents.

Here, we describe the automation of islet stimulation on a microfluidic system designed to operate using vacuum-based fluidic transport. Pneumatic valves[19] were incorporated to gate the flow of perfusion solutions to the islet chamber and allow for selective stimulant delivery. During the testing of the device, spikes in the flow were observed that were attributed to the closing of the valves. Implementation of fluidic capacitors was found to be essential for reducing these spikes and producing smooth responses. The integration of these fluidic components allowed for automated perfusion and stimulation of single murine islets allowing the profiling of dynamic glucose-stimulated insulin secretion.

Materials and methods

Chemicals and reagents

Sodium chloride, calcium chloride, sodium hydroxide, ethylenediaminetetraacetic acid (EDTA), Tween 20, bovine serum albumin (BSA), and ammonia were from EMD Chemicals (San

*[a]Department of Chemistry & Biochemistry, Florida State University, 95 Chieftain Way, Tallahassee, FL 32306, USA. E-mail: mroper@fsu.edu; Tel: +1 850-644-1846
[b]Program in Molecular Biophysics, Florida State University, 95 Chieftain Way, Tallahassee, FL 32306, USA*
†Electronic supplementary information (ESI) available. See DOI: https://doi.org/10.1039/d2an01985j

Diego, CA). Dextrose, RPMI 1640 containing L-glutamine and 11 mM glucose, gentamicin, and fetal bovine serum (FBS) were from Thermofisher Scientific (Waltham, MA). *Collagenase P* (*from Clostridium histolyticum*) was acquired from Roche Diagnostics (Indianapolis, IN). Monoclonal anti-insulin antibody (Ab) was purchased from Meridian Life Science, Inc. (Saco, ME). Cy5-labeled insulin (Ins*) was prepared in-house, as previously described.[20] All other reagents were purchased from Sigma-Aldrich (St Louis, MO) unless noted otherwise. All solutions were made with Milli-Q (Millipore, Bedford, MA) 18 MΩ cm ultrapure water and filtered using 0.2 μm nylon syringe filters (Pall Corporation, Port Washington, NY). Immunoassay reagents (Ins* and Ab) were prepared in TEAT-40 (pH 7.4) composed of 25 mM tricine, 40 mM NaCl, 1 mM EDTA, 0.1% Tween-20 (w/v) and 1 mg mL^{-1} BSA. Insulin standards were prepared in balanced salt solution (BSS) (pH 7.4) which consisted of 125 mM NaCl, 2.4 mM $CaCl_2$, 1.2 mM $MgCl_2$, 5.9 mM KCl, 25 mM tricine, with pH adjusted to 7.4 with NaOH. An additional 1 mg mL^{-1} BSA was added to the BSS with different levels of glucose as stated in the text.

Isolation of islets of langerhans

Islets of Langerhans were isolated from male CD-1 mice (25–40 g) using a protocol approved by the Animal Care and Use Committee at Florida State University (protocol 202000078). Isolated islets were incubated in RPMI-1640 media containing 10% FBS, 1% penicillin and streptomycin, and 0.1% gentamicin at 37 °C and 5% CO_2. Before use in experiments, an islet was washed with pre-warmed BSS containing 3 mM glucose.

Microfluidic device fabrication

A 4-layer glass/polymer microfluidic device was fabricated by photolithography and wet chemical etching. The first 2-layers formed the fluidic layer and were composed of an etched glass layer thermally bonded to a blank piece of glass. In the etched glass layer, channels from two perfusion reservoirs extended for 5 mm, followed by a gap of 1 mm, which continued for a further 30 mm to the 300 μm diameter islet chamber. Two 600 μm diameter holes were drilled on either side of the 1 mm gap. All channel dimensions were 25 × 50 μm (depth × width at the bottom) as measured with an SJ-410 surface profiler (Mitutoyo Corp., Aurora, IL). Inlets to all channels were made with a 0.02″ diamond drill bits (Industrial Power Tool and Abrasives, NY). This etched piece was then thermally bonded to a blank piece of glass at 640 °C for 8 h. Oval valve seats were etched into a different piece of glass to a dimension of 2.0 × 1.0 mm × 20 μm (length × width × depth) and irreversibly bonded to a ~250 μm thin PDMS film (HT-6240, Bisco Silicones, Rogers Corp., Chandler, AZ). This valve layer was reversibly bonded to the fluidic layer with the valve seat bridging the 1 mm gap, allowing fluidic passage from the inlet reservoir to the islet chamber when the valve was opened. Fluidic reservoirs (IDEX Health and Science, Oak Harbor, WA) were bonded to the microfluidic device to hold perfusion and assay reagents. Fluidic capacitors were fabricated as described in the text.

Microfluidic device operation

Solenoid valves (Model A00SC232P, Parker Hannifin Corp, Cleveland, OH) were used to direct 1.5 PSI or 5 inHg vacuum from a dry piston pump (Welch 2522B-01, Gardner Denver, Monroe, LA) to the microfluidic valve seats to close or open them, respectively. The solenoids were controlled *via* TTL actuation from a PCI-6009 data acquisition card (National Instruments, Austin, TX). Fluidic transport in the device was driven by a syringe pump (Harvard Apparatus, Holliston, MA) and a 500 μL gastight syringe (Hamilton Company Inc., Reno, NV) connected to the common outlet of the device using 0.02″ ID × 0.06″ OD Tygon tubing (Cole-Parmer North America, Vernon Hills, IL) through a finger-tight fitting (IDEX Health and Science). This pump, operated in withdrawal mode at 0.90 μL min^{-1} pulled fluid equally from the perfusion channel and the two immunoassay reagent channels through the mixing channel to the detection window before exiting the device *via* the outlet.

Fluorescence anisotropy detection system

Fluorescence anisotropy was measured as has been described elsewhere.[21,22] Briefly, the microfluidic device was placed on the stage of an Eclipse TS-100 microscope (Nikon Instruments Inc., Melville, NY). Fluorescence excitation was from a 25 mW 635 nm laser (Coherent Inc. Santa Clara, CA) attenuated to 2 mW with a neutral density filter (Thorlabs Inc., Newton, NJ) and coupled into a multimode fiber-optic bundle (Ceramoptec, Sunnyvale, CA) by an achromatic fiber port collimator (PAF2S-7A, Thorlabs). The light was then fed into a telescoping lens tube (SM1NR1, Thorlabs) where it was collimated by an in-tube achromatic doublet (AC254-080-A-ML, Thorlabs) and randomly polarized by a quartz-wedge achromatic depolarizer (DPU-25-A, Thorlabs). This beam entered the back of the microscope and was linearly polarized with a linear polarizer (WP25M-VIS, Thorlabs), reflected by a dichroic mirror (XF2035, Omega Optical Inc., Brattleboro, VT) into a 40×, 0.6 NA objective (Nikon) which then focused the beam into the detection point on the microfluidic device.

Emitted fluorescence was collected with the same objective, transmitted through the dichroic, and directed into a two-channel microscope photometer (Horiba Scientific, Piscataway, NJ) where the light passed through a 665 nm long-pass filter (HQ665LP, Chroma Technology Corp., Bellows Falls, VT), and a 635 nm notch filter (ZET635NF, Chroma Technology Corp.). The emission was then passed through a polarizing beamsplitter cube (PBS101, Thorlabs) and split into parallel and perpendicular polarized components (with respect to the excitation polarization). Afterward, each polarized component was passed through a complementary linear polarizer before impinging on separate photomultiplier tubes (PMTs) (R10699, Hamamatsu Photonics, Middlesex, NJ). Data from both PMTs were collected at 1000 Hz with a USB 6009 DAQ card (National Instruments) and converted to anisotropy using a program

written in-house (LabView, National Instruments). All anisotropy traces were smoothed by a 10 000-point moving boxcar average in MATLAB (MathWorks, Natick, MA).

Data analysis

The concentrations of Ins* and Ab in the reservoirs were 75 nM, which resulted in a final concentration of 25 nM for both after online mixing. To perform a calibration, insulin concentrations ranging from 0 to 1800 nM in BSS were placed in the perfusion reservoirs and anisotropy was measured for 5 min. The average anisotropy for the 5 min was plotted against the corresponding insulin concentration and data were fitted to a four-parameter logistic curve using Origin 9.0 (OriginLab, Northampton, MA, USA). For presentation, calibration curves are shown as the change in anisotropy (Δr) taken as relative to that measured at 0 nM insulin. All error bars are ±1 standard deviation (SD) unless otherwise noted. The limit of detection (LOD) was calculated as the concentration of insulin required to decrease anisotropy to a value lower than 3 times the SD of the blank. For insulin secretion measurements, the calibration function was used to convert anisotropy values to insulin concentrations and subsequently normalized by the flow rate through the islet chamber. Unless otherwise noted, all experiments were performed at 37 °C as previously described.[21,22]

Results and discussion

The use of vacuum pressure for fluidic transport in microfluidic systems has been well-reported in the literature.[15–18,23] Vacuum-based systems allow for passive control across multiple channels using a single pressure source, without the need for multiple connections that are often required in other pressure-driven flow systems. Eliminating the need for multiple connections greatly reduces the complexity and volume of the overall system, thereby leading to simple devices with low reagent usage, as well as fast response and analysis times. However, independent manipulation of flow from multiple channels in a vacuum-driven system is challenging due to the passive nature of the control. In this work, we describe the automation of islet stimulation on a microfluidic system with vacuum-based fluidic transport using integrated pneumatic valves that allowed for selective stimulant delivery to an islet on the device. Integrated pneumatic valves are widely used in flow gating and can be readily automated using computer-assisted programming.[19,24–26] This automation in addition to reducing the chances of contamination can also lead to more complex fluidic systems without sacrificing the ease of vacuum-based fluid control.

Microfluidic device characterization

A top view of the microfluidic design is illustrated in Fig. 1A. Fluid transport in the device was driven by a syringe pump operating in withdrawal mode attached to the outlet reservoir. Because of the passive nature of this fluid transport mechanism, flow was pulled equally from all channels in the device,
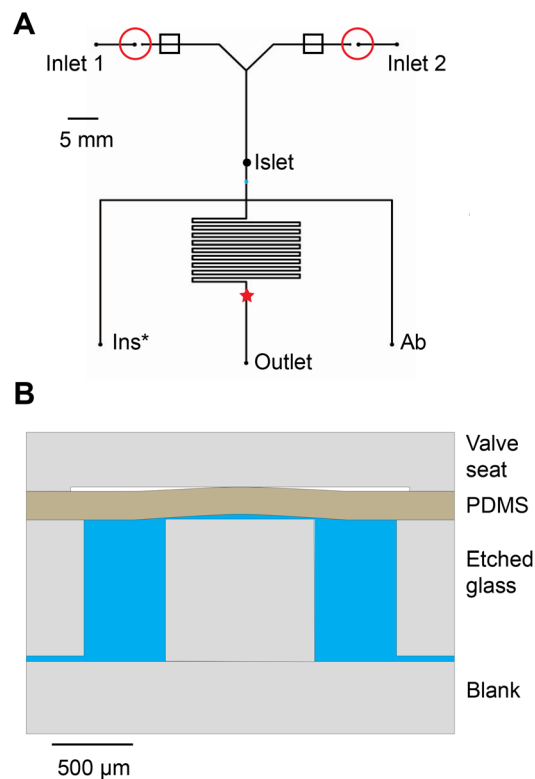

Fig. 1 Microfluidic system. (A) Top view of the microfluidic design used in the experiments. A syringe pump operating in withdrawal mode at the outlet reservoir pulled the perfusion solutions through valves (red circles) and past the closed islet chamber where it collected the secretions. The perfusate then met with Ins* and Ab and traveled through the 25 cm mixing channel prior to detection at the point shown by *. The locations of the fluidic capacitors are shown by the open boxes. (B) Conceptualized side-on view of a 4-layer valve used to control flow from inlets 1 and 2 is shown. The "valve seat" and "blank" layers are not to scale for ease in visualization. Applied vacuum evacuated the top displacement chamber and pulled up the PDMS layer to open the valve.

including the two perfusion reservoirs above the islet chamber (inlets 1 and 2). To direct the flow from only one of the reservoirs at a time, 4-layer valves (Fig. 1B) were incorporated into each of the perfusion channels. These valves were straightforward to incorporate into the glass device and because they were upstream of the islet chamber, there was no concern of the islet secretions traveling through the valves and being diluted by their volume.

At any point during an experiment, one of the valves was open while the other was closed. The open valve allowed fluid to flow from that particular inlet to the islet chamber and transported the islet secretions to the mixing cross where it met with the Ab and Ins* that were also being pulled. As the channel lengths of the Ab, Ins*, and islet chamber (to one of the perfusion inlets) were all 38.5 mm and etched to the same depth and width, the flow rates from the three were the same. We did not observe an effect of the valve on the resistance of the perfusion lines as evidenced by equal flow coming from the three channels (Fig. S1†).

Paper

To visualize the automated delivery of liquid, inlets 1 and 2 were filled with a yellow and green food coloring solution, respectively, and the flow was imaged downstream of the two valves where the channels joined. As seen in Fig. 2A, when the valve to inlet 1 was open and that to inlet 2 was closed, the green dye was pulled into the device. When the valves were switched, the flow from inlet 1 was terminated and yellow dye

Fig. 2 Initial valve opening protocol. (A) Visualization of flow control with food coloring. Top, green food coloring flowed towards the islet chamber when the valve on inlet 1 was open and the valve on inlet 2 was closed. Bottom, yellow food coloring flowed from inlet 2 towards the islet chamber when the valves were switched. (B) The PMT signal is shown when Cy5 and buffer were placed in inlets 1 and 2, respectively, and detection occurred after the islet chamber. The valves to the two inlets were alternately opened and closed every 60 s. The upward spikes in the signal occurred when the valve to the Cy5 inlet was closed while the downward spikes occurred when the valve to the buffer inlet was closed.

was pulled from inlet 2. For a more quantitative analysis of the flow dynamics, inlet 1 was filled with 1 µM Cy5 and inlet 2 with buffer and the detection point was placed in the microfluidic channel just after the islet chamber. Both perfusion channels were primed to ensure that they were filled to the valve seat before data collection started. The valves gating the buffer and Cy5 were then alternately opened and closed every 60 s for 600 s. The observed response (Fig. 2B) followed the expected trend with fluorescence intensity rising from baseline to a threshold intensity. In like fashion, a decay of the fluorescence intensity was observed when the flow was switched back to buffer from Cy5. This trend was consistent throughout the duration of the experiment. However, at the point of valve actuation, sharp spikes and dips in the fluorescence intensity were observed when the valves were closed. This was thought to be a result of an increased flow of the respective fluid when a valve was closed, with spikes corresponding to closure of the Cy5 valve and dips corresponding to closure of the buffer valve.

To reduce these spikes, the valve seats were positioned closer to the inlet reservoir (5 mm) as compared to the islet chamber (30 mm) to ensure lower fluidic resistance between the valve seat and the inlet reservoirs, and higher fluidic resistance from the valve seat to the islet chamber. We hypothesized that any pulse arising from the closing of the pneumatic valves would be directed preferentially toward the inlet reservoirs due to the lower resistance. Additional designs were tested with even lower channel resistances from the inlet reservoirs to the valve seat by increasing the channel width to 500 µm from the initial 50 µm. However, none of these designs eliminated the spikes when the valves closed.

A microfluidic device integrated with a fluidic capacitor

To eliminate the hydrodynamic pressure spikes following valve closure, the use of elastomeric fluidic capacitors[27] was explored. Capacitors are made by bonding a deformable elastomer over a portion of the fluidic channel which allows the elastomer to expand and deform in response to a pressure pulse.[27,28] These components have been used, for example, in frequency-specific flow control in microfluidic devices[27] and to produce pressure stimuli that mimic heartbeats in a microfluidic cell culture platform.[29]

The possibility of incorporating one capacitor before the islet chamber for both perfusion inlets was considered. This would simplify the fabrication process, but it would increase the volume, and increase the time, required to change stimulants when the valves were switched. Therefore, two capacitors, one on each perfusion inlet channel, were fabricated near each valve (open boxes in Fig. 1A). Fig. 3A shows a to-scale schematic of an integrated fluid capacitor with a valve. To incorporate these capacitors into the microfluidic device, a 1.1 mm diameter hole was drilled in each perfusion channel 8.5 mm after each of the valve seats. These drilled holes were sealed with the PDMS film that was used as the valve layer. To ensure that the PDMS could expand and temporarily accommodate the volume emptied from the valve seats, a ~5 mm diameter circle
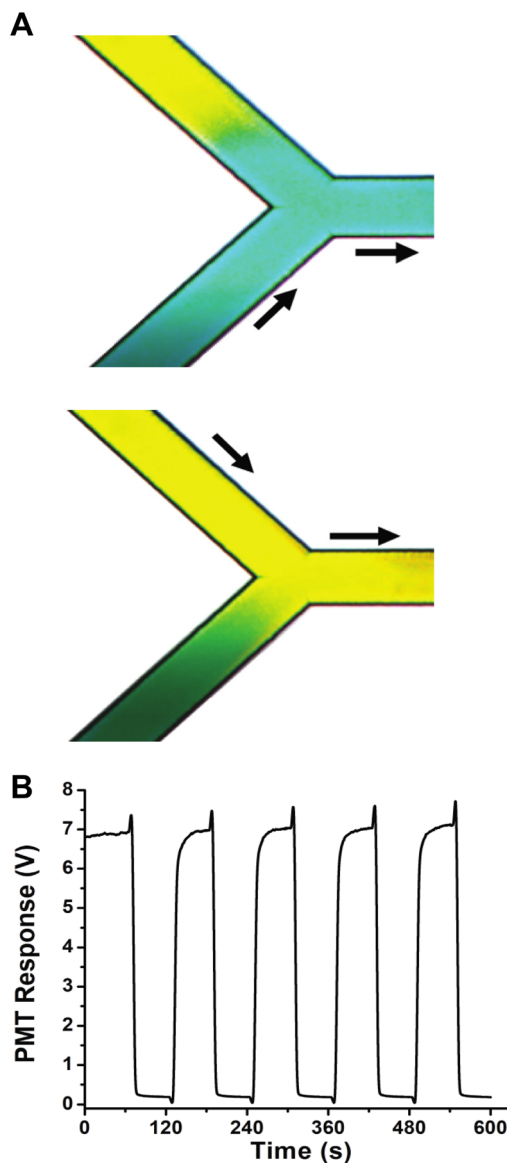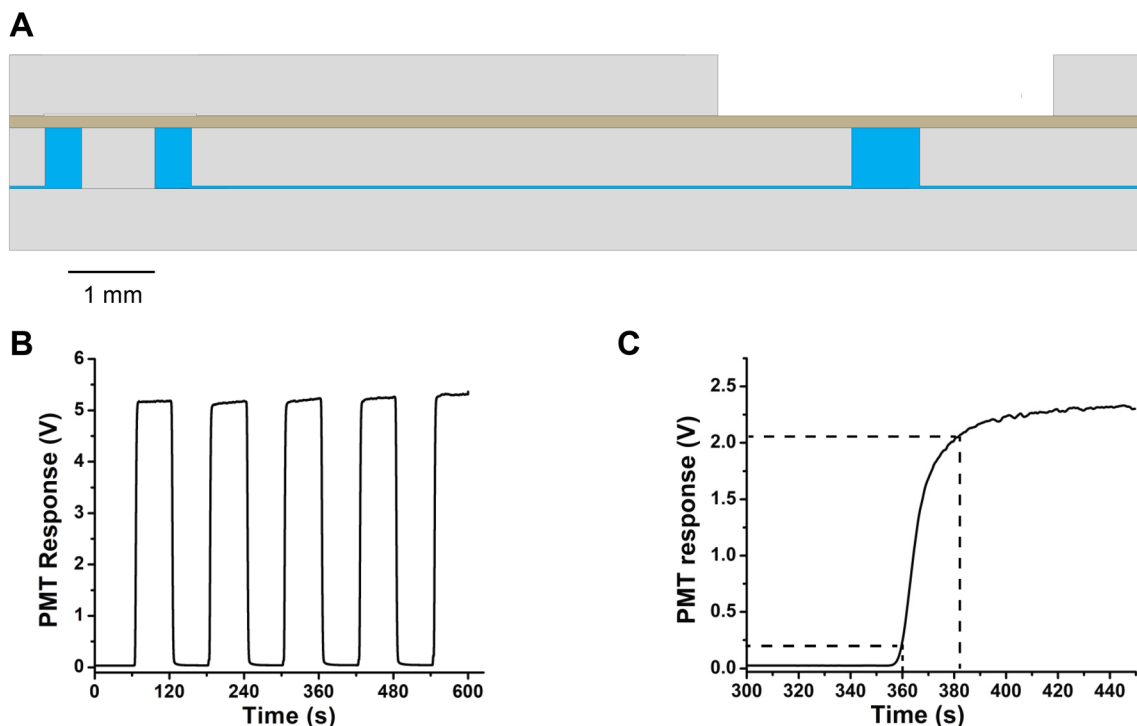
Fig. 3 Fluidic capacitors. (A) Side view of a valve and fluidic capacitor showing the 1.1 mm diameter drilled hole in the fluid layer as well as the 5 mm milled portion of the top glass layer. (B) PMT response profile from 60 s switches between the valves directing flow from the buffer and Cy5 inlet reservoirs on the microfluidic device with integrated fluidic capacitors. (C) PMT response at the immunoassay detection point after a valve switch from buffer to Cy5. The dashed lines indicate the times for determination of t_D and t_R.

was milled out above the 1.1 mm diameter hole in the topmost layer of the device that contained the valve seats. The flow dynamics in this device were tested by repeating the experiment described earlier by alternating the delivery of 1 μM Cy5 and buffer from inlet reservoirs 1 and 2 in 60 s pulses and fluorescence measured just after the islet chamber. As seen in Fig. 3B, the average RSD of the PMT response from the five regions of Cy5 detection was 0.2% indicating a smooth flow during the valve openings and closings.

Once the pressure spike was reduced, the overall microfluidic system was further characterized. The delay and response times (t_D and t_R, respectively) of the device were determined by delivering Cy5 pulses, similar to those described above, but detecting at the end of the immunoassay mixing channel (indicated by * in Fig. 1A). The t_D is defined as the time to reach 10% of the final PMT response while t_R was the time required for the fluorescence intensity to rise from 10% to 90% of the final PMT response after a flow switch from buffer to Cy5. The experimental result for this evaluation was 60 ± 1 s and 22 ± 1 s for t_D and t_R, respectively, across 5 Cy5 pulses (Fig. 3C).

Insulin measurements

Using the optimized system, calibration curves were obtained by loading standard insulin solutions into the perfusion reservoirs and delivering through the on-chip valves and islet chamber. At the immunoassay mixing cross, the standard insulin solution met with the immunoassay reagents and tra-

veled the 25 cm mixing channel before fluorescence anisotropy detection. A representative calibration curve is shown in Fig. 4A. The anisotropy showed a progressive decrease as the insulin concentration increased. This result agrees with standard fluorescence anisotropy competitive immunoassays in which the decrease in measured anisotropy is a result of the increased amount of free Ins* and decreased amount of Ab–Ins* complex with increasing insulin concentration.[21,22,30,31] Because the free Ins* rotates faster than the Ab–Ins*, the average anisotropy of the solution decreases. The delivery of insulin standards through the valves had no adverse effect on the immunoassay as the RSD of all points were less than 1%, similar to other reported anisotropy systems that did not use valves.[21,22,32–34] The LOD was calculated to be 10 nM, a concentration low enough to demonstrate the feasibility of utilizing this device to measure insulin secretion from single murine islets.

To test islet responsiveness to glucose, single murine islets were challenged with an increase in glucose while insulin was measured. To perform these experiments, inlets 1 and 2 were filled with 3 and 11 mM glucose in BSS, respectively. To prime the device, both perfusion valves were opened, and flow through the device was initiated. After 40 min, the valve to the 11 mM glucose solution was closed while the valve to the 3 mM glucose solution was left open to ensure that the islet chamber was filled with this solution before islet loading. After 20 min, the valve to the 3 mM glucose solution was
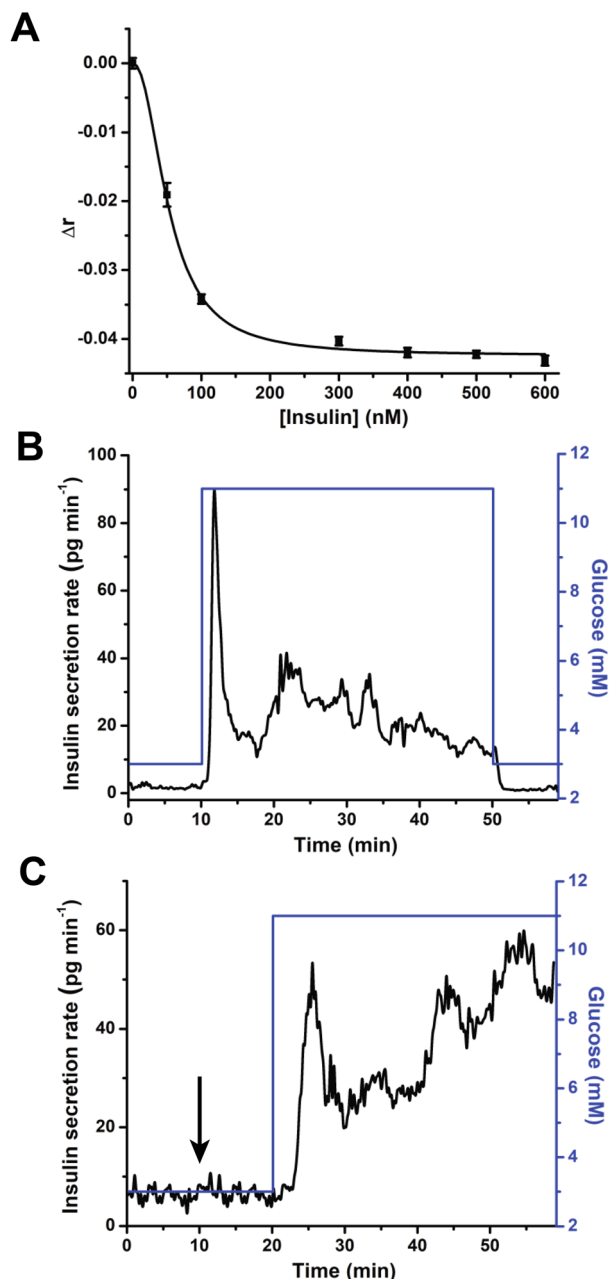
Fig. 4 Insulin immunoassay calibration curve. (A) Representative calibration curve of the change in anisotropy (Δr) as a function of insulin concentration. The final concentrations of both Ab and Ins* were 25 nM. The points are the average of 300 s of anisotropy measurements while error bars are ± 1 SD. (B) Representative insulin secretion profile (black line, left y-axis) from a single murine islet with the delivered glucose concentration (blue, right y-axis). A rapid increase in insulin secretion was observed following exposure to the elevated glucose level and a return to non-stimulatory glucose concentration resulted in the return of the insulin secretion rate to basal levels. (C) Control experiment where a murine islet was stimulated with 3 mM glucose for the first 10 min. At 10 min (shown by arrow), the valves switched to deliver the same glucose concentration for an additional 10 min after which the 3 mM glucose solution was removed from the device and replaced with 11 mM glucose to initiate insulin release.

closed and the syringe pump stopped. A single murine islet was loaded into the islet chamber which was then sealed with PCR tape. The valve to the 3 mM glucose solution was opened and flow was re-initiated by starting the syringe pump. Another 10 min was allowed before anisotropy measurements began. The stimulation protocol was to perfuse with 3 mM glucose for 10 min, followed by 11 mM glucose for 40 min, and a return to 3 mM for a final 10 min.

Fig. 4B shows a representative profile from a single murine islet obtained on this integrated device. This insulin release profile followed a pattern previously described for rodent islets with a characteristic burst of insulin in the first 10–15 min followed by a period of sustained secretion.[8–11,13,14,21,22,35–41] Insulin secretion rates returned to basal levels with the return to 3 mM glucose. Fig. S2A–G† shows additional insulin response profiles from single islets. As a comparison, insulin release was measured from islets without fluidic capacitors to examine how the pressure pulse would affect their secretion profiles. Single murine islets were loaded into a device and a similar perfusion protocol was applied. While increases in insulin were observed after stimulation with high glucose, the profiles showed an increase in the baseline directly after the valves switched between low and high glucose (Fig. S3†). Removal of the sharp fluidic pulses by the capacitors correlates with the disappearance of the increase in baseline. It was unclear why the spikes would result in an increase in the baseline secretion, but the secretion profiles from the device with the integrated capacitors are more similar to literature reports as compared to the ones without the capacitors.

Control experiments were run to verify that the actuation of the pneumatic valves was not affecting the secretion profiles. In these experiments, the two perfusion inlet reservoirs were filled with 3 mM glucose. The experiment began with one of the valves closed and the other open allowing 3 mM glucose to be delivered to an islet for 10 min. After this time, the valves were switched to allow flow from the other inlet for another 10 min. After 20 min, data recording was temporarily paused, the syringe pump was stopped, and the valve was closed to allow for the replacement of the 3 mM glucose solution in inlet 2 with 11 mM glucose. The valve for inlet 2 was then opened and the syringe pump started to allow 11 mM glucose to flow through to stimulate the islet while the measurement was resumed and continued for another 40 min. Fig. 4C shows the response and that switching from one 3 mM glucose solution to another did not result in a significant change in insulin response even though a valve switch was performed at 10 min, indicated with a downward arrow. The only noticeable change to the insulin secretion rate occurred after delivering the stimulatory 11 mM glucose solution. This control experiment was repeated as shown in Fig. S2-H† with similar results.

Conclusions

In this work, on-chip pneumatic valves were incorporated to automate the delivery of stimulants to an islet on a microflui-

dic device and demonstrated its utility for real-time measurement of insulin secretion from single islets. The initial designs of the device exhibited short-lived pressure spikes initiated by the rapid emptying of the valve seat volume when the valves were closed. This challenge was resolved through the incorporation of in-line fluid capacitors which acted as pressure dampeners and helped to smoothen out the fast flow pulse to give way to a smooth response profile. While only two stimulants were shown here, the methodology is applicable to even higher numbers of stimulants and to higher numbers of islet chambers. Therefore, the development of this system opens a path to higher throughput systems where the use of multiple valves can be used to direct the flow of different stimuli to on-chip organoids.

Author contributions

Damilola I. Adeoye: Investigation, writing – original draft and writing – review & editing. Yao Wang: Resources and writing – review and editing. Joshua J. Davis: Resources and writing – review and editing. Michael G. Roper: Investigation, resources, funding acquisition and writing – review & editing.

Conflicts of interest

The authors declare no conflicts of interest.

Acknowledgements

References

1 G. Da Silva Xavier, *J. Clin. Med.*, 2018, **7**, 54.
2 S. G. Straub and G. W. G. Sharp, *Diabetes/Metab. Res. Rev.*, 2002, **18**, 451–463.
3 J.-C. Henquin, N. Ishiyama, M. Nenquin, M. A. Ravier and J.-C. Jonas, *Diabetes*, 2002, **51**, S60–S67.
4 J. E. Gerich, *Diabetes*, 2002, **51**, S117–S121.
5 A. L. Glieberman, B. D. Pope, D. A. Melton and K. K. Parker, *Diabetes*, 2021, **70**, 347–363.
6 Y. Wang, J. F. Lo, J. E. Mendoza-Elias, A. F. Adewola, T. A. Harvat, K. P. Kinzer, D. Lee, M. Qi, D. T. Eddington and J. Oberholzer, *Bioanalysis*, 2010, **2**, 1729–1744.
7 F. R. Castiello, K. Heileman and M. Tabrizian, *Lab Chip*, 2016, **16**, 409–431.
8 P. W. Jin, N. Rousset, A. Hierlemann and P. M. Misun, *Front. Bioeng. Biotechnol.*, 2021, **9**, 674431.
9 P. M. Misun, B. Yesildag, F. Forschler, A. Neelakandhan, N. Rousset, A. Biernath, A. Hierlemann and O. Frey, *Adv. Biosyst.*, 2020, **4**, 1900291.
10 T. Hori, K. Yamane, T. Anazawa, O. Kurosawa and H. Iwata, *Biomed. Microdevices*, 2019, **21**, 91.
11 G. Lenguito, D. Chaimov, J. R. Weitz, R. Rodriguez-Diaz, S. A. K. Rawal, A. Tamayo-Garcia, A. Caicedo, C. L. Stabler, P. Buchwald and A. Agarwal, *Lab Chip*, 2017, **17**, 772–781.
12 M. Nourmohammadzadeh, Y. Xing, J. W. Lee, M. A. Bochenek, J. E. Mendoza-Elias, J. J. McGarrigle, E. Marchese, Y. Chun-Chieh, D. T. Eddington, J. Oberholzer and Y. Wang, *Lab Chip*, 2016, **16**, 1466–1472.
13 T. Schulze, K. Mattern, E. Früh, L. Hecht, I. Rustenbeck and A. Dietzel, *Biomed. Microdevices*, 2017, **19**, 47.
14 D. Lee, Y. Wang, J. E. Mendoza-Elias, A. F. Adewola, T. A. Harvat, K. Kinzer, D. Gutierrez, M. Qi, D. T. Eddington and J. Oberholzer, *Biomed. Microdevices*, 2012, **14**, 7–16.
15 K. S. Deal and C. J. Easley, *Anal. Chem.*, 2012, **84**, 1510–1516.
16 L. A. Godwin, M. E. Pilkerton, K. S. Deal, D. Wanders, R. L. Judd and C. J. Easley, *Anal. Chem.*, 2011, **83**, 7166–7172.
17 C. J. Easley, J. V. Rocheleau, W. S. Head and D. W. Piston, *Anal. Chem.*, 2009, **81**, 9086–9095.
18 Y. Wang, D. I. Adeoye, Y. J. Wang and M. G. Roper, *Anal. Chim. Acta*, 2022, **1212**, 339942.
19 W. H. Grover, A. M. Skelley, C. N. Liu, E. T. Lagally and R. A. Mathies, *Sens. Actuators, B*, 2003, **89**, 315–323.
20 C. Guillo and M. G. Roper, *J. Chromatogr. A*, 2011, **1218**, 4059–4064.
21 J. E. Adablah, Y. Wang, M. Donohue and M. G. Roper, *Anal. Chem.*, 2020, **92**, 8464–8471.
22 A. M. Schrell, N. Mukhitov, L. Yi, J. E. Adablah, J. Menezes and M. G. Roper, *Anal. Methods*, 2017, **9**, 38–45.
23 Y. Zhao, D. Chen, Z. Xu, T. Li, J. Zhu, R. Hu, G. Xu, Y. Li, Y. Yang and M. Liu, *Anal. Chem.*, 2023, DOI: **10.1021/acs.analchem.2c05320**.
24 K. W. Oh and C. H. Ahn, *J. Micromech. Microeng.*, 2006, **16**, R13–R39.
25 R. Zhong, M. Wang and B. Lin, *Electrophoresis*, 2023, DOI: **10.1002/elps.202200185**.
26 C. Quintard, E. Tubbs, J.-L. Achard, F. Navarro, X. Gidrol and Y. Fouillet, *Biosens. Bioelectron.*, 2022, **202**, 113967.
27 D. C. Leslie, C. J. Easley, E. Seker, J. M. Karlinsey, M. Utz, M. R. Begley and J. P. Landers, *Nat. Phys.*, 2009, **5**, 231–235.
28 B. Mosadegh, T. Bersano-Begey, J. Y. Park, M. A. Burns and S. Takayama, *Lab Chip*, 2011, **11**, 2813–2818.
29 J. Wu, Y. Hirai, K.-I. Kamei, T. Tsuchiya and O. Tabata, *Electron. Commun. Jpn.*, 2019, **102**, 41–49.
30 M. Cobb and S. Gotcher, *Am. J. Med. Technol.*, 1982, **48**, 671–677.
31 W. B. Dandliker and V. A. de Saussure, *Immunochemistry*, 1970, **7**, 799–828.
32 A. M. Schrell, N. Mukhitov and M. G. Roper, *Anal. Chem.*, 2016, **88**, 7910–7915.
33 N. Mukhitov, J. E. Adablah and M. G. Roper, *Islets*, 2019, **11**, 21–32.
34 A. L. Glieberman, B. D. Pope, J. F. Zimmerman, Q. Liu, J. P. Ferrier Jr., J. H. R. Kenty, A. M. Schrell, N. Mukhitov,

K. L. Shores, A. B. Tepole, D. A. Melton, M. G. Roper and K. K. Parker, *Lab Chip*, 2019, **19**, 2993–3010.

35 J. G. Shackman, G. M. Dahlgren, J. L. Peters and R. T. Kennedy, *Lab Chip*, 2005, **5**, 56–63.

36 J. F. Dishinger, K. R. Reid and R. T. Kennedy, *Anal. Chem.*, 2009, **81**, 3119–3127.

37 S. N. Patel, M. Ishahak, D. Chaimov, A. Velraj, D. LaShoto, D. W. Hagan, P. Buchwald, E. A. Phelps, A. Agarwal and C. L. Stabler, *Sci. Adv.*, 2021, **7**, eaba5515.

38 G. Lenguito, D. Chaimov, J. R. Weitz, R. Rodriguez-Diaz, S. A. K. Rawal, A. Tamayo-Garcia, A. Caicedo, C. L. Stabler, P. Buchwald and A. Agarwal, *Lab Chip*, 2017, **17**, 772–781.

39 J. Hu and C. J. Easley, *Anal. Chem.*, 2017, **89**, 8517–8523.

40 L. Yi, X. Wang, R. Dhumpa, A. M. Schrell, N. Mukhitov and M. G. Roper, *Lab Chip*, 2015, **15**, 823–832.

41 B. Bandak, L. Yi and M. G. Roper, *Lab Chip*, 2018, **18**, 2873–2882.